Draft version September 19, 2016
Preprint typeset using LaTeX style emulateapj v. 12/16/11

COSMOLOGICAL CONSTRAINTS FROM THE REDSHIFT DEPENDENCE OF THE GALAXY ANGULAR 2-POINT CORRELATION FUNCTION

Xiao-Dong Li,
School of Physics, Korea Institute for Advanced Study, 85 Heogiro, Dongdaemun-gu, Seoul 130-722, Korea

Cheng Cheng,
Kavli Institute for Theoretical Physics China, Institute of Theoretical Physics, Chinese Academy of Sciences, Zhong Guan Cun Street 55#, Beijing, 100190, P.R. China and
University of Chinese Academy of Sciences, P.R. China

Changbom Park,
School of Physics, Korea Institute for Advanced Study, 85 Heogiro, Dongdaemun-gu, Seoul 130-722, Korea

Hyunbae Park, Cristiano G. Sabiu,
Korea Astronomy and Space Science Institute, Daejeon 305-348, Korea

Juhan Kim[1],
Center for Advanced Computation, Korea Institute for Advanced Study, 85 Hoegi-ro, Dongdaemun-gu, Seoul 130-722, Korea and
School of Physics, Korea Institute for Advanced Study, 85 Heogiro, Dongdaemun-gu, Seoul 130-722, Korea

and

Stephen Appleby, Sungwook E. Hong
School of Physics, Korea Institute for Advanced Study, 85 Heogiro, Dongdaemun-gu, Seoul 130-722, Korea

Draft version September 19, 2016

ABSTRACT

We propose to use the redshift of the shape of galaxy angular 2-point correlation function (2pCF) to constrain cosmology. The method is a continue of our series of works (Li et al. 2014, 2015, 2016) probing the redshift dependence of Alcock-Paczynski effect and volume effect. A wrongly adopted cosmology result in redshift-dependent mis-scaling in the constructed galaxy distribution, which leads to redshift-dependent rescaling in the measured angular 2pCF. We test our method on the HR4 mock galaxies having 457, 406, 352, 206 and 228 million galaxies at redshfits 0, 0.5, 1, 1.5, 2, and find the redshift evolution of the scaling of angular 2pCF is sensitive to the adopted cosmological parameters and relatively insensitive to the gravitational growth of structure, the galaxy bias, and the redshift space distortion. Analyzing redshift evolution of the shape of 2pCF on scales $5h^{-1}$Mpc $\leq r_{\perp} \leq 40h^{-1}$Mpc we derive tight constraints on Ω_m and w. Our method is complementary to current works using 2pCF to constrain cosmological parameters. The method could be applicable to future photometric surveys of DES, LSST to derive tight cosmological constraints.

Keywords: large-scale structure of Universe — dark energy — cosmological parameters

1. INTRODUCTION

The discovery of cosmic acceleration (Riess et al. 1998; Perlmutter et al. 1999) implies the existence of a “dark energy” component in the Universe or the breakdown of Einstein’s gravity theory on cosmological scales. The theoretical explanation and observational probe of cosmic acceleration has attracted tremendous effort in the last two decades and are still far from well understood or accurately measured (Weinberg 1989; Li et al. 2011; Weinberg et al. 2013).

In an effort to probe the cosmic expansion history the large scale structure (LSS) surveys enable measurements of two geometrical quantities, the angular diameter distance D_A and the Hubble factor, H. If they were precisely measured as a function of redshift, tight constraints can be placed on cosmological parameters, e.g. the matter density Ω_m and the equation of state (EoS) of dark energy w.

As one geometrical effect of cosmological parameters on LSS, when an incorrect cosmological model is assumed for the coordinate transformation from redshift space to comoving space, geometric distortions are produced in the constructed galaxy distribution. These distortion include the “volume effect” which is the mis-scaling of the size of structures, and the Alcock-Paczynski (AP) effect, the shape distortion induced by the fact that distances along and perpendicular to the line of sight are fundamentally different.

Various statistically methods has been proposed to measure these effects. The AP effect has been proposed to measure through the clustering of galaxies (Ballinger Peacock & Heavens 1996; Matsubara & Suto 1996) which has been applied to a series of LSS surveys (Outram et al. 2004; Blake et al. 2011; Chuang & Wang 2012; Reid et al. 2012; Beutler et al. 2013; Linder et al. 2014; Song et al. 2014; Jeong et al. 2014; Sutter et al. 2014; López-Corredoira 2014; Alam et al. 2016; Beutler et al. 2016;

[1] Corresponding Author: kjhan@kias.re.kr

Sanchez et al. 2016), the alternative approaches using the symmetry properties of galaxy pairs (Marinoni & Buzzi 2010; Jennings et al. 2011; **?**) and cosmic voids (Ryden 1995; Lavaux & Wandelt 2012; Sutter et al. 2014; Mao et al. 2016). Methods proposed able to probe the volume effect include the number counting of galaxy clusters (Press & Shechter 1974; Viana & Liddle 1996) and topology (Park & Kim 2010), the BAO scale (Eisenstein et al. 1998; Blake & Glazebrook 2003; Seo & Eisenstein 2003), and the shape of 2pCF and power spectrum (Sáchez et al. 2006; Sánchez et al. 2009).

In Li et al. (2014, 2015, 2016) we proposed a series of methods to probe the geometric information encoded in the LSS data. We make use of the fact that the AP or volume effect commonly introduce redshift-dependent geometric distorion in the LSS, which can be distinguished from the other effects such as the redshfit space distortion (RSD). RSD arises because the radial distances of galaxies are inferred from redshifts which is contaminated by the pecular motion of galaxies, leading to apparent anisotropy even if the adopted cosmology is correct (Ballinger Peacock & Heavens 1996). RSD is the usually main caveats for probe geometry using LSS, and we found it can be largerly avoid by focusing on the the redshift dependence of the anisotropy.

Li et al. (2014) proposed used the *galaxy density gradient field* to characterize the anisotropies in LSS and tested the idea on Horizon Run 3 (HR3) N-body simulations (Kim et al. 2011), showing the redsift evolution of the gardient field can be used to infer unbiased constraints cosmological parameters and is insensitive to RSD. The same topic was revisited in Li et al. (2015), but using the statistical tool of *galaxy two-point correlation function* (2pCF) as a function of angle, $\xi(\mu)$. When incorrect cosmological parameters are adopted, the shape of $\xi(\mu)$ appears anisotropic due to the AP effect, and the amplitude is shifted by the change in comoving volume; both effects have significant redshift dependence. The RSD effect, although significantly distorting $\xi(\mu)$, exhibits much less redshift evolution compared to the effect coming from incorrectly adopted cosmologies. The method was applied to BOSS DR12 galaxies (Li et al. 2016) to probe the redshift dependent of AP effect and lead to tight cosmological constraints.

We developed a method measuring the redshift of the shape of galaxy angular correlation function to constrain cosmology. A wrongly adopted cosmology result in redshift-dependent mis-scaling in the constructed galaxy distribution, which leads to redshift-dependent change in the angular 2pCF shape. The signal is sensitive to the adopted cosmological parameters and relatively insensitive to the gravitational growth of structure, the galaxy bias, and the RSD effect. We test our method on the HR4 mock galaxies having hundreds of million galaxies at redshfits 0-2. Analyzing redshift evolution of the shape of 2pCF on scales $5-40h^{-1}$Mpc, we derive tight constraints on Ω_m and w.

In this paper we continue our series of work and probe to use the angular correlation function as a statistical tool to probing the volume effect in the angular direction. A wrongly adopted cosmology result in redshift-dependent mis-scaling in the constructed galaxy distribution, which shifts apparent scale of the clustering patterns; this manifests itself as a redshift-dependent rescaling of the measured angular correlation function. We find this signal is sensitive to the adopted cosmological parameters and relatively insensitive to the gravitational growth of structure, the galaxy bias, and the RSD effect. We test our method on the HR4 mock galaxies. The method can be applied to current and future LSS surveys, especially, the photometric surveys such as DES and LSST which probe a large amount of galaxies and the large redshift error will not quite affect the angular 2pCF measurement.

The outline of this paper proceeds as follows. In §2 we briefly review the nature and consequences of the geometric distortion in LSS when performing coordinate transforms in a cosmological context. In §3 we describe the mock galaxies produced from N-body simulations which are used to test our methodology. The methodology is presented in §4. We conclude in §6.

2. VOLUME EFFECT IN A NUTSHELL

In this section we briefly introduce the scaling effect caused by wrongly assumed cosmological parameters. A more detailed description has been provided in Li et al. (2014, 2015, 2016).

Suppose that we are probing the size of some objects in the Universe. We measure its redshift span Δz and angular size $\Delta\theta$, then compute its sizes in the radial and transverse directions using the following formulas

$$\Delta r_{\parallel} = \frac{c}{H(z)}\Delta z, \quad \Delta r_{\perp} = (1+z)D_A(z)\Delta\theta, \tag{1}$$

where H is the Hubble parameter and D_A is the angular diameter distance. In the particular case of a flat universe composed by a cold dark matter component and a constant EoS dark energy component, they take the forms of

$$\begin{aligned} H(z) &= H_0\sqrt{\Omega_m a^{-3} + (1-\Omega_m)a^{-3(1+w)}}, \\ D_A(z) &= \frac{1}{1+z}r(z) = \frac{1}{1+z}\int_0^z \frac{dz'}{H(z')}, \end{aligned} \tag{2}$$

where $a = 1/(1+z)$ is the cosmic scale factor, H_0 is the present value of Hubble parameter and $r(z)$ is the comoving distance.

In case wrong values of Ω_m and w are adopted, the inferred $\Delta r_{\parallel}$ and $\Delta r_{\perp}$ are wrong, resulting in wrong estimation in the object's shape (AP effect) and size (volume effect). These effects and their cosmological consequences have been investigated in Li et al. (2014, 2015, 2016).

In this paper we focus on the mis-estimation of the angular size $\Delta r_{\perp}$. The ratio of mis-estimation is

$$\alpha_{\perp} \equiv \frac{\Delta r_{\perp,\rm wrong}}{\Delta r_{\perp,\rm true}} = \frac{D_{A,\rm wrong}}{D_{A,\rm true}}, \tag{3}$$

where "true" and "wrong" denote the values of D_A in the true cosmology and wrongly assumed cosmologies, respectively.

An illustration is provided in the left panels of Figure 1. Suppose that the true cosmology is a flat ΛCDM with present matter ratio $\Omega_m = 0.26$ and standard dark energy EoS $w = -1$. If we were to distribute a series of perfect squares at various distances ranging from 500 Mpc/h to 3 000 Mpc/h, and an observer located at the origin were to measure their redshifts and infer the sizes of the squares using the distance-redshift relations of four incorrect cosmologies

$$\text{(i)}.\ \Omega_m = 0.40,\ w = -1.0,$$

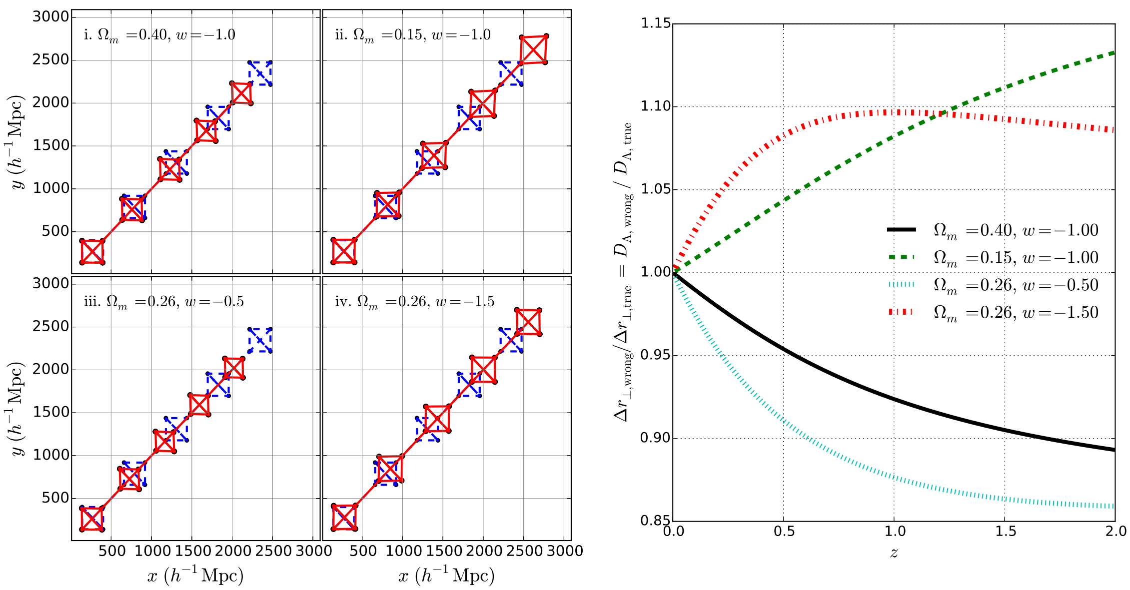

Figure 1. The scaling in four wrongly assumed cosmologies ..., assuming a true cosmology of $\Omega_m = 0.26$, $w = -1$. Left panel shows a series objects distributes as five perfect squares, measured by an observer located at the origin. Their true positions and shapes are plotted in blue dashed lines. The observer measures the redshifts of these objects, adopts the wrong cosmologies to compute the distance, and obtains wrong results (the red solid lines). Right panel shows the mis-estimation of angular diameter distance when the wrong cosmologies are adopted.

$$(\mathrm{ii}).\ \Omega_m = 0.15,\ w = -1.0,$$
$$(\mathrm{iii}).\ \Omega_m = 0.26,\ w = -0.5,$$
$$(\mathrm{iv}).\ \Omega_m = 0.26,\ w = -1.5,$$

as a result, the shapes of the squares appear distorted (AP effect), and their sizes are wrongly estimated (volume effect). Cosmological models (i,iii) yield to compressed size (in both angular and LOS direction), and the degree of compression increases with increasing distance;

The mis-estimation of angular size, $\Delta r_{\perp,\mathrm{wrong}}/\Delta r_{\perp,\mathrm{true}}$, are displayed in the right panel of Figure 1. All cosmologies, $\Delta r_{\perp,\mathrm{wrong}}/\Delta r_{\perp,\mathrm{true}}$ evolves a lot in the redshift range $0 < z < 2$. As an example, when adopting the quintessence cosmology $\Omega_m = 0.26$, $w = -0.5$, the angular size is underestimated by 8.9%, 12.3%, 13.6%, 14.1% at $z = 0.5, 1, 1.5, 2$.

In sum, as a consequence of incorrectly adopted cosmologies, the size of the objects is mis-estimated and the magnitude of mis-estimation depends on the redshift. In this paper we use the galaxy angular 2pCF to probe the mis-estimation of angular size $\Delta r_{\perp,\mathrm{wrong}}/\Delta r_{\perp,\mathrm{true}}$.

3. THE SIMULATION DATA

We test the method using the mock galaxy samples produced by the Horizon Run 4 (HR4) N-body simulation (Kim et al. 2015; Hong et al. 2016).

HR4 was made within a cube of volume $(3.15\,h^{-1}\mathrm{Gpc})^3$ using 6300^3 particles with mass $m_p \simeq 9 \times 10^9 h^{-1}\mathrm{M}_\odot$. The simulation adopted the second order Lagrangian perturbation theory (2LPT) initial conditions at $z_i = 100$ and a WMAP5 cosmology $(\Omega_b, \Omega_m, \Omega_\Lambda, h, \sigma_8, n_s) = (0.044, 0.26, 0.74, 0.72, 0.79, 0.96)$ (Komatsu et al. 2011).

Mock galaxies are produced from the simulation based on a modified one-to-one correspondence scheme (Hong et al. 2016). The most bound member particles (MBPs) of simulated halos are adopted as tracers of galaxies. The merger timescale is computed to get the lifetime of merged halos. Merger trees of halos are constructed by tracking their MBPs from $z = 12$ to 0; when a merger event occurs, the merger timescale is computed using the formular of Jiang et al. (2008) to determine when the satellite galaxy is completely disrupted.

The resulting mock galaxies was found to reproduce the 2pCF of SDSS DR7 volume-limited galaxy sample (Zehavi et al. 2011) very well (Hong et al. 2016). The mock galaxies shows a similar finger of god (FOG) feature (Jackson 1972) as the observation. The projected 2pCF of the mock and observational samples agree within 1σ CL on scales greater than 1 h^{-1}Mpc.

In this analysis we use snapshot data of HR4 galaxies at $z = 0, 0.5, 1, 1.5, 2$. Setting a minimal halo mass of $3 \times 10^{11} h^{-1}\mathrm{M}_\odot$, we select 457, 406, 352, 206 and 228 million mock galaxies at the five redshifts, corresponding to a number density of 1.46, 1.30, 1.13, 0.98 and 0.73 in unit of $10^{-2} h^3\mathrm{Mpc}^{-3}$, respectively. By applying a uniform mass cut, at higher redshift we are selecting less galaxies with larger galaxy bias.

As an illustration, Figure 2 displays the 2D distribution of a subsample of mock galaxies in five redshifts, with x, y coordinates computed using the "correct" values of cosmological parameters $\Omega_m = 0.26$, $w = -1$ (left panels) and a wrong set of cosmological parameters $\Omega_m = 0.05$, $w = -1.5$ (right panels), respectively.

When the correct cosmology is adopted the cosmic scale is correctly estimated in five redshifts. The only factor leads to evolution of galaxy distribution with redshift is the gravitational growth of structure. With the decreasing the redshift, we clearly see how the clusters and filaments form and grow. On the other hand, when the wrong cosmology is adopted, there is an artifical scaling of scales in the constructed map. The separations among galaxies are overestimated by 25.6%, 47.3%, 62.2%, 71.7% at redshifts of 0.5, 1.0, 1.5, 2.5, leading to a clear evolution of the sizes of structures with redshift.

The growth of structure leads to growth of clustering strength of structures on all scales, while the volume effect maintain the clustering pattern and uniformly rescale all the structures. Their imprints on the large scale structure is different and should be distinguishable in the statistical analysis. In the following, we show that they affect the angular correlation function measurements in different ways, and can be easily separated.

The growth of structure also make the size of structures evolves with redshift. In the next subsection we will discuss how to distinguish these two effects in the galaxy angular 2pCF.

4. METHODOLOGY

We use the angular 2pCF as a statistical tool to probe the volume effect. The galaxy 2pCF as a function of galaxy separation in the angular direction, $\omega(r_\perp)$, is computed for snapshot data of mock galaxies at five redshifts. We adopt the Landy-Szalay estimator (Landy & Szalay 1993),

$$\omega(r_\perp) = \frac{DD - 2DR + RR}{RR} \ , \tag{4}$$

where DD is the number of galaxy–galaxy pairs, DR the number of galaxy-random pairs, and RR is the number of random–random pairs, all separated by a distance defined by $r_\perp \pm \Delta_{r_\perp}$ where we choose $\Delta_{r_\perp} = 1h^{-1}$Mpc. The random catalogue consists of unclustered points uniformly distributed in a same size box. In an effort to reduce the statistical variance of the estimator, we use 50 times as many random points as we have galaxies.

Considering the large number of galaxies and random points the 2pCF is computed part by part in subsamples with size of 1575 h^{-1}Mpc$\times$1575 h^{-1}Mpc$\times$105 h^{-1}Mpc. The Z direction with thickness 105 h^{-1}Mpc is treated as the radial direction (the r direction) and the X-Y directions with each of width $1575h^{-1}$ Mpc are the angular plane. For our simulation box size we can have 120 such subsamples. The average of the measurements in all subsamples is adopted as the 2pCF of the whole sample, while the covariances of them are adopted as the covariance matrix after multiplying a factor of $1/\sqrt{119}$.

4.1. *Galaxy angular 2pCF: amplitude and shape at different redshifts*

The upper-left panel of Figure 3 displays the angular 2pCF measured from HR4 mock galaxies. We multiply ω by the separation $r_\perp$ to have similar amount of statistical uncertainty on all scales.

At different redshifts, we see large evolution in the amplitude of $\omega(r_\perp)$. The amplitude of 2pCF is proportional to the clustering strengh which is affected by the gravitational growth of structures and the bias of the galaxies. The amplitude is highest at $z=0$ where the large scale structures experienced most gravitational growth, and also gets higher at $z>1$ with increasing redshift as a reason of more biased galaxies at higher redshift.

Different from the large variation of amplitude among the different redshifts, the shape of $r_\perp\omega$ maintains similar at all redshifts; it always peaks at $r\sim 9h^{-1}$Mpc and monotonically drops at larger or smaller scales. The only exception is the small enhancement at $r\lesssim 2h^{-1}$Mpc, which is caused by the non-linear growth of structures on small scales and is much more significant at lower redshfit.

In order to directly compare the shape of 2pCF at different redshifts, in the middle panel of Figure 3 we show the $r_\perp\omega$ normalized by the overall amplitude within $5h^{-1}$Mpc $< r < 50h^{-1}$Mpc (here after $\hat\omega_{r_\perp}$):

$$\hat\omega_{r_\perp} \equiv \frac{r_\perp\omega(r_\perp)}{\int_{r_{\perp,\rm min}}^{r_{\perp,\rm max}} r_\perp\omega(r_\perp)dr_\perp/(r_{\perp,\rm max}-r_{\perp,\rm min})}, \tag{5}$$

where we choose $r_{\perp,\rm min} = 5h^{-1}$ Mpc, $r_{\perp,\rm max} = 40h^{-1}$ Mpc in this analysis. Scales of $r_{\perp,\rm min} < 5h^{-1}$ Mpc are affected by non-linear growth of strucutre, the mis-estimation of whose contribution may lead to systematic errors in the derived cosmological constraints. On scales larger than $40h^{-1}$ Mpc it is may be possible to have precise analytically modelling the shape of the 2pCF (Salvador et al. 2014, 2016) which should be able to extract more cosmological information than our method (although out method should is also applicable).

The nice overlapping of the five redshift results justify the small evolution of shape with redshift. In the right panel, we further show the residual evolution of $\hat r_\perp\omega$ at high redshifts with respect to $z=0$. There is only 1-4% relative enhancement at $r<10h^{-1}$Mpc, and $<1.5\%$ relative suppression at $r>25h^{-1}$Mpc. The trend is monotonic with redshift.

There is one point should be emphasized here. In real observations we are observing *different* objects in different redshfit shells. To mimick this we comparing slices of different redshifts at *different* locations. As an exammple, if at $z=0$ we take $\hat\omega_{r_\perp}$ measured within $0h^{-1}$Mpc $<$ $Z<105h^{-1}$Mpc, at higher redshifts we then adopt measurement within $105h^{-1}$Mpc $< Z < 210h^{-1}$Mpc for a comparision. If simply comparing the 2pCF of a *same* subsample of galaxies at different redshifts, one would significantly underestimate the statistical undertainty of $\delta\hat{\omega_{r_\perp}}$ by ignoring the cosmic variance. The error bars and covariance are always estimated in this way to take the cosmic variance into consideration.

As shown by Figure 2, the gravitational growth of strucutre enhance the clustering strengh of structures on all scales; here it manifests itself as an enhanced amplitude of 2pCF at low redshift. The shape of 2pCF, which represents the *relative strength of clustering among different scales*, maintain similar with redshift except the non-linear scales of $r_\perp < 5h^{-1}$Mpc.

4.2. *Galaxy angular 2pCF: Cosmological Effect*

The measured angular correlation function of galaxies with positions constructed using the wrong cosmology $\Omega_m=0.05$, $w=-1.5$ is displayed in the lower panels of Figure 3. The mis-scaling uniformly shifts clustering patterns on all scales, lead to a wrong estimation of $\hat\omega_{r_\perp}$ related with the correct one as

$$\hat\omega_{r_\perp,\rm wrong}(r) = \hat\omega_{r_\perp,\rm correct}(\alpha_\perp r), \tag{6}$$

a simple consequence of the phenomenon that clustering patterns at distance r now appears on $\alpha_\perp r$. The redshift evolution of $\alpha_\perp$ leads to redshfit evolution of shape.

The change in shape as well as the redshift evolution is displayed in the middle panel. The upscaling of comoving distance lead to a stretched shape. With the increasing of redshift, the peak location is shifted from $9h^{-1}$Mpc to $15h^{-1}$Mpc at $z=2$, as a result of the fact that the angular separation is upscaled by 71.7%. Correspondingly,

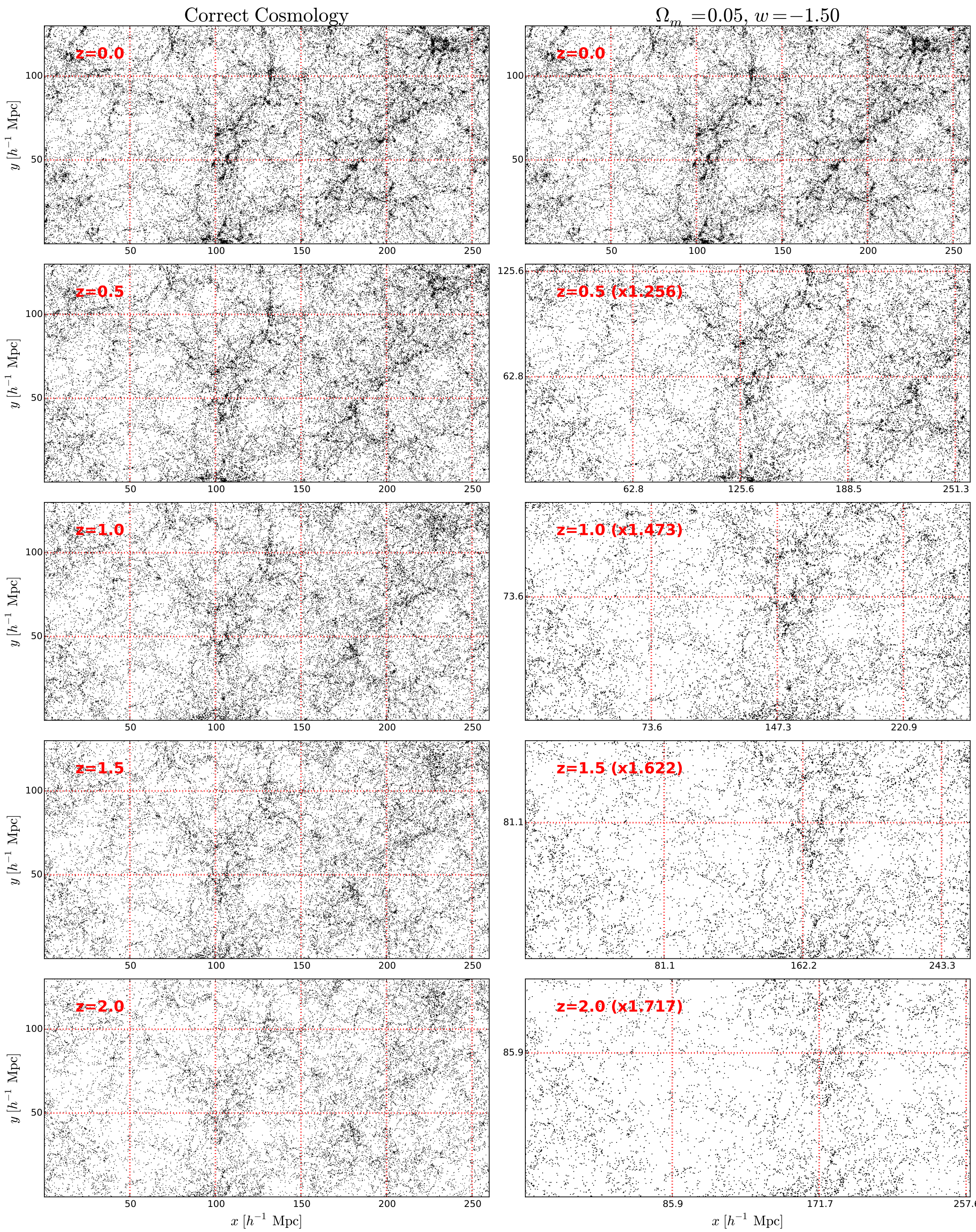

Figure 2. blah

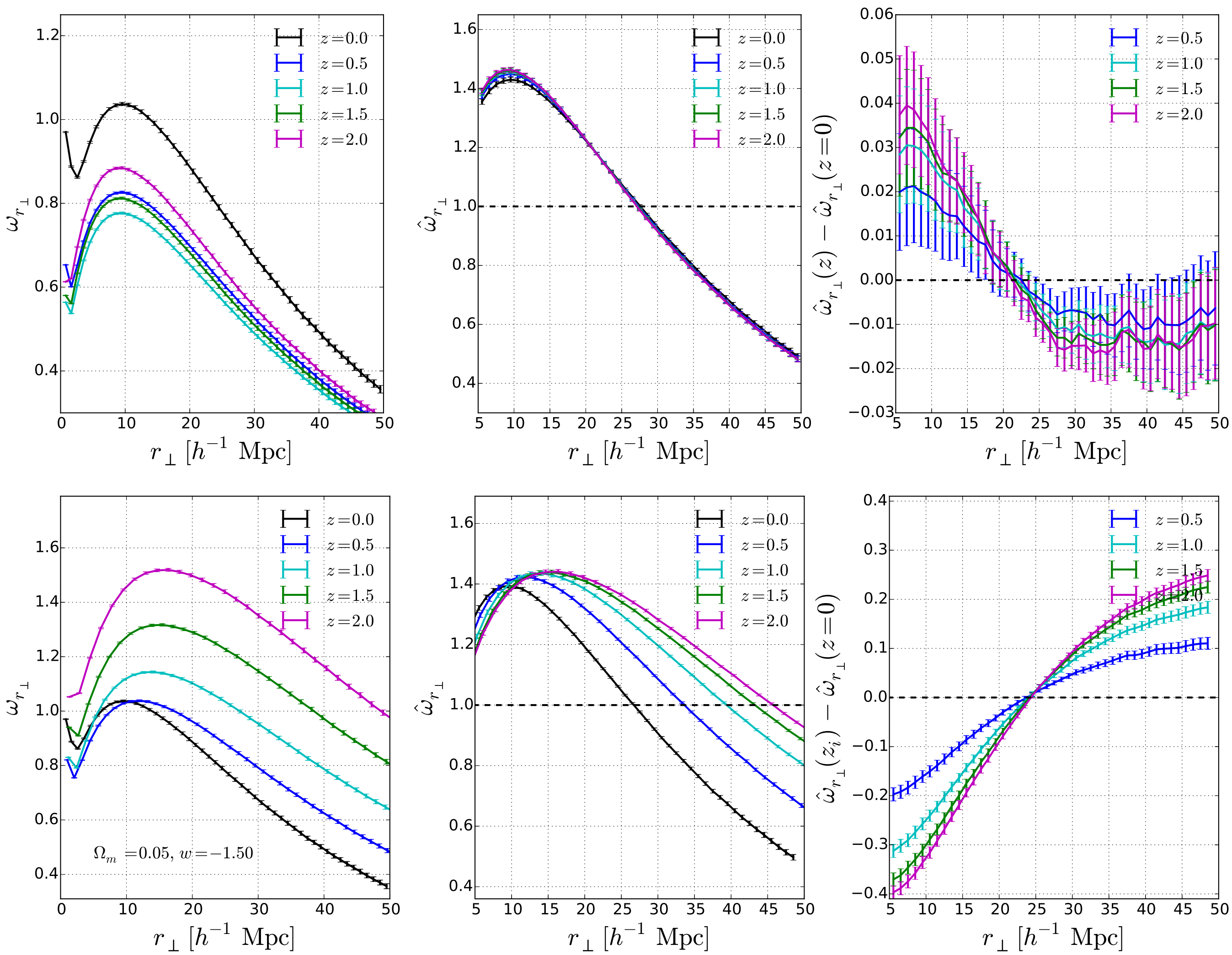

Figure 3. 2pCF at different redshfits.

the right panel shows that, compared with $\hat{\omega}_{r_\perp}$ at $z=0$ there is a 20-40% change at higher redshifts.

The mis-scaling not only changes the of the 2pCF but also modifies its amplitude. as shown in the left panel, due to the stretch of scale the amplitude is enhanced at higher redshifts; the higher the redshift, the more the enhancement.

Although the change of amplitude could be a more significant consequence of wrong cosmology than the alteration of shape, it is mixed with other factors; the growth of structure and a larger galaxy bias can also lead to a stronger clustering and thus an enhanced amplitude of 2pCF. In the analysis to extract cosmological information, we just make use of the redshift evolution of the 2pCF shape, which is less affected by factors of structure growth and galaxy bias.

4.3. *Systematic effects*

Sec. 4.1 shows that $\hat{\omega}_{r_\perp}$ measured from a set of constant mass cut samples at different redshifts is close to each other. The gravitational growth of structure will not have a large impact on $\hat{\omega}_{r_\perp}$ on scales $\gtrsim 5h^{-1}$ Mpc. The other factors may introduce redshift evolution of the clustering of measured galaxies include the redshift space distortion (RSD), galaxy bias, redshift error, and other properties of galaxies, such as the mass, morphology, color, concentration. Here we test two "major" systematical effects, the galaxy bias and the RSD effect.

4.3.1. *Galaxy Bias*

Galaxies are biased tracers of dark matter field; more massive galaxies reside in regions with higher density contrast. In large scale structure surveys, the bias of the galaxy sample is an important fator affecting on the clustering properties of the sample.

We check the effect of galaxy bias on $\hat{\omega}_{r_\perp}$. The upper panels of Figure 4 displays the 2pCF measured from galaxies within a $3175\times3175\times105$ $(h^{-1}\mathrm{Mpc})^3$ volume, taken from the $z=0$ snapshot. Four values of minimal mass limits, $3\times10^{11}M_\odot$, $1\times10^{12}M_\odot$, $4\times10^{12}M_\odot$ and $1\times10^{13}M_\odot$, are imposed to create three samples with different galaxy bias. The measured angular 2pCF are displayed.

The different mass cuts result in large variation in the amplitude of the 2pCF (left panel), while the shape of the 2pCF remains less affected (middle panel). Compared with the sample of $M>3\times10^{11}M_\odot$, samples with mass limits of $1\times10^{12}M_\odot$, $4\times10^{12}M_\odot$ and $1\times10^{13}M_\odot$ have amplitude of 2pCFs enhanced by 10%, 50% and 100%, while the change in $\hat{\omega}_{r_\perp}$ is only 0.5%, 2% and 4%. So the effect of galaxy bias is much avoided by utilizing the shape of the 2pCF rather than the amplitude.

4.3.2. *Redshift Space Distortion*

The galaxy peculiar velocity contributes to the observed redshift and distorted the inferred galaxy radial position, known as the redshift space distortion. It is the major systematics in our previous works (Li et al. 2014, 2015, 2016) where we derive cosmological constraints from the redshift evolution of the 3D galaxy distribution.

The effect of RSD is expected to be much milder in this work. The angular positions of the galaxies is not shifted by RSD at all; the only effect of RSD come in the procedure of sample preparation. The galaxies observed in a survey are split into shells of subsamples with different redshift ranges for the purpose 2pCF measurement. RSD disortes the galaxy redshift and as a result some galaxies (especially those close to the boundaries of shells) could be classified to wrong redshift shells.

The lower panel of Figure 4 displays the RSD effect on 2pCF. To have the effect of RSD we shift the radial coordinates of galaxies according to the relation

$$\Delta z = (1+z)\frac{v_{\mathrm{Z}}}{c}, \tag{7}$$

where v_{LOS} is the galaxy peculiar velocity in the radial direction. This lead to mis-classfication of some galaxies when we split the box into slices.

Comparing the plot with Figure 3 one clearly see the effect of RSD. The amplitude of measured 2pCF is enhanced by $\sim10\%$ in case of considering the RSD effect. The slop of $\hat{\omega}_{r_\perp}$ slightly suppressed. While the redshift evolution of $\hat{\omega}_{r_\perp}$ is still small... Although the pattern is a little modified... So RSD is not a big issue here... **after anna jobs finished we have better plots and re-revise this section**

Similar to RSD, redshift errors of galaxies (typically 0.02 for photometric survey) also results in fuzzy boundaries of shells and mis-classfication of galaxies. This effect should also be properly quantified in real observations.

4.4. *Likelihood Analysis*

We design the likelihood function to quantify the redshift evolution of $\hat{\omega}_{r_\perp}$. A cosmology resulting in smaller evolution is considered to be more likely the correct one. The procedure here is very similar to what we did in Li et al. (2014, 2015, 2016). We comapre the high redshift $\hat{\omega}_{r_perp}$ and the lowest redshift measurement:

$$\chi^2 \equiv \sum_{i=2}^{n_z}\sum_{j_1=1}^{n_r}\sum_{j_2=1}^{n_r}\mathbf{p}(z_i,r_{j_1})(\mathbf{Cov}_i^{-1})_{j_1,j_2}\mathbf{p}(z_i,r_{j_2}), \tag{8}$$

where n_z is the number of redshifts which is 5 in this analysis, n_r is number of binning in $\hat{\omega_{r_\perp}}(r_\perp)$, which is 35 since we have $r_\perp$ bins with width $1h^{-1}$Mpc in a range of $5h^{-1}\mathrm{Mpc}\le r\le 40h^{-1}$Mpc. $\mathbf{p}(z_i,r_j)$ is the redshift evolution of the angular correlation function shape with systematic effects subtracted

$$\mathbf{p}(z_i,r_j) \equiv\ \delta\hat{r_\perp}\omega(z_i,z_1,r_j) - \delta\hat{r_\perp}\omega_{\mathrm{sys}}(z_i,z_1,r_j) \tag{9}$$

$\mathbf{Cov}_i$ is the covariance matrix estimated from the $\mathbf{p}(z_i,r_j)$ measured from 120 subsamples. As mentioned before, for a robust estimation of covariance matrix, we always compare slices at different locations to include the cosmic variance.

The covariance matrix inferred from a finite number of samples is always a biased estimate of the true matrix (Hartlap et al. 2006). This can be corrected by rescaling the inverse covariance matrix as

$$\mathbf{Cov}^{-1}_{ij,\mathrm{Hartlap}} = \frac{N_s-n_r-2}{N_s-1}\mathbf{Cov}^{-1}_{ij}, \tag{10}$$

where $N_s=120$ is the number of mocks used in covariance estimation. For the options of this analysis the rescaling is as large as 1.43. In the case that one have 2 000 mocks the rescaling is less than 1.02.

Figure 5 displays the 2pCF and the likelihood values in case of adopting the four wrong cosmologies of Figure 1. For the cosmologies $\Omega_m=0.4, w=-1$ and

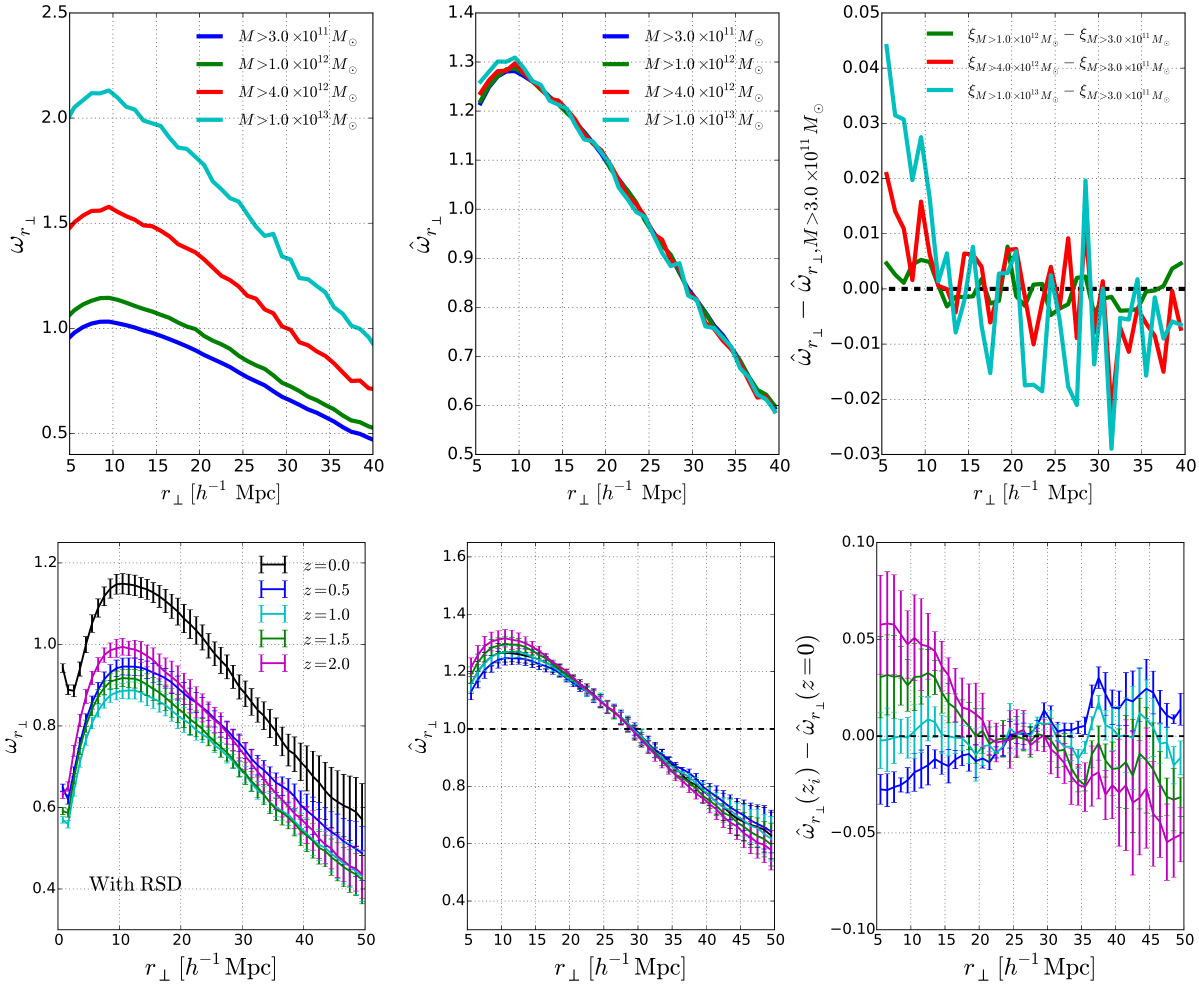

Figure 4. Systematic effects.

$\Omega_m = 0.26, w = -0.5$, the compression of structure shift the large scale clustering patterns into small scales, and also becomes more significant at higher redshift. We get 2pCFs with steeper slope and the higher redshift the steeper. For cosmologies $\Omega_m = 0.15, w = -1$ and $\Omega_m = 0.26, w = -1.5$, the stretch of structure leads to shallower slope of $\hat{\omega_{r_\perp}}$ and the higher the redshift the shallower. In all cosmologies we have significant detection of redshift evolution. We computed the χ^2 values according to Equation 8, and found these cosmological parameters are strongly disfacored at $\gtrsim 30\sigma$ CL.

5. COSMOLOGICAL CONSTRAINT

We constrain Ω_m and w through Bayesian analysis (Christensen et al. (2001); also see Lewis & Bridle (2002); Li et al. (2016)). We assue the likelihood takes the form

$$\mathcal{L} \propto \exp\left[-\frac{\chi^2}{2}\right] \tag{11}$$

and scan the parameter space in $\Omega_m - w$ plane to obtain the 68.3% and 97.4% CL regions. The result is displayed in Figure 6.

We get tight constraint on the two paramters. The 2σ contour lies within the region $0.23 < \Omega_m < 0.285$, $-1.1 < w < -0.9$. The thin shape of contour means, when combining with the another observational data with different direction of degeneracy (e.g. CMB), very tight combined constraint can be obtained. In case of fixing one parameter at its best-fit value and infer the statistical uncertainty of the other one, one will obtain 1σ uncertainty of $\delta\Omega_m \approx 0.002, \delta w \approx 0.01$.

6. CONCLUDING REMARKS

We developed a method measuring the redshift of the shape of galaxy angular correlation function, $\hat{\omega}_{r_\perp}$, to constrain cosmology. A wrongly adopted cosmology result in redshift-dependent mis-scaling in the constructed galaxy distribution, which leads to redshift-dependent rescaling of $\hat{\omega}_{r_\perp}(r_\perp)$. The signal is sensitive to the adopted cosmological parameters and relatively insensitive to the gravitational growth of structure, the galaxy bias, and the RSD effect. We test our method on the HR4 mock galaxies having 457, 406, 352, 206 and 228 million galaxies at redshfits 0, 0.5, 1, 1.5, 2; analyzing redshift evolution of the shape of 2pCF on scales $5h^{-1}\mathrm{Mpc} \leq r_\perp \leq 40h^{-1}\mathrm{Mpc}$ we derive tight constraints on Ω_m and w.

The angular correlation function is adopted as a statistical tool to probing the scaling effect in the angular direction. One can also use the 2D 2pCF as a function of both angular and radial scale to fully probe the scaling effect in 3D galaxy distribution.

There are already works using the shape of angular 2pCF to constrain cosmology by directly comparing the theoretical 2pCF to the observed one (Salvador et al. 2014, 2016). While our method just utilize the fact the

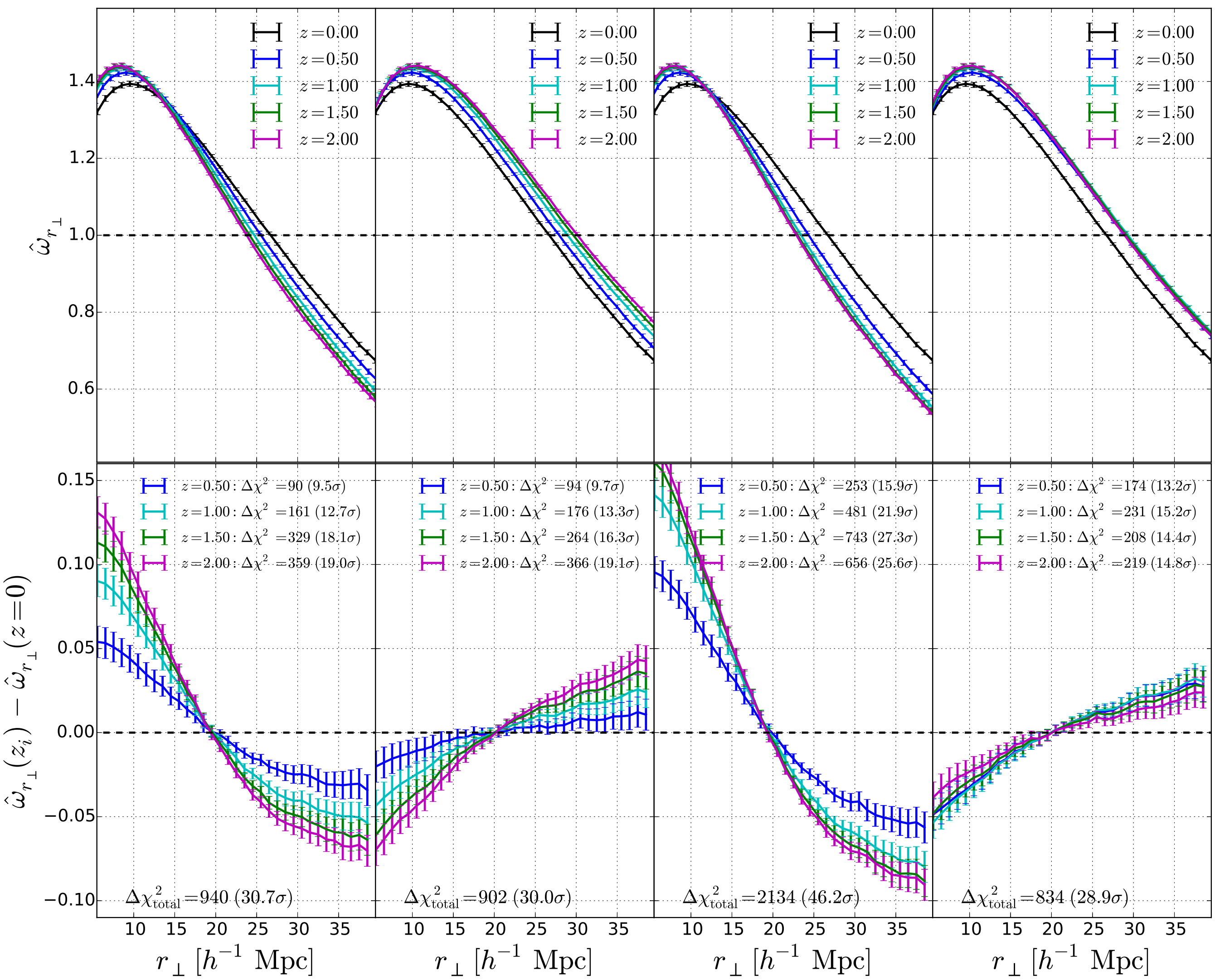

Figure 5. 2pCF in cosmologies.

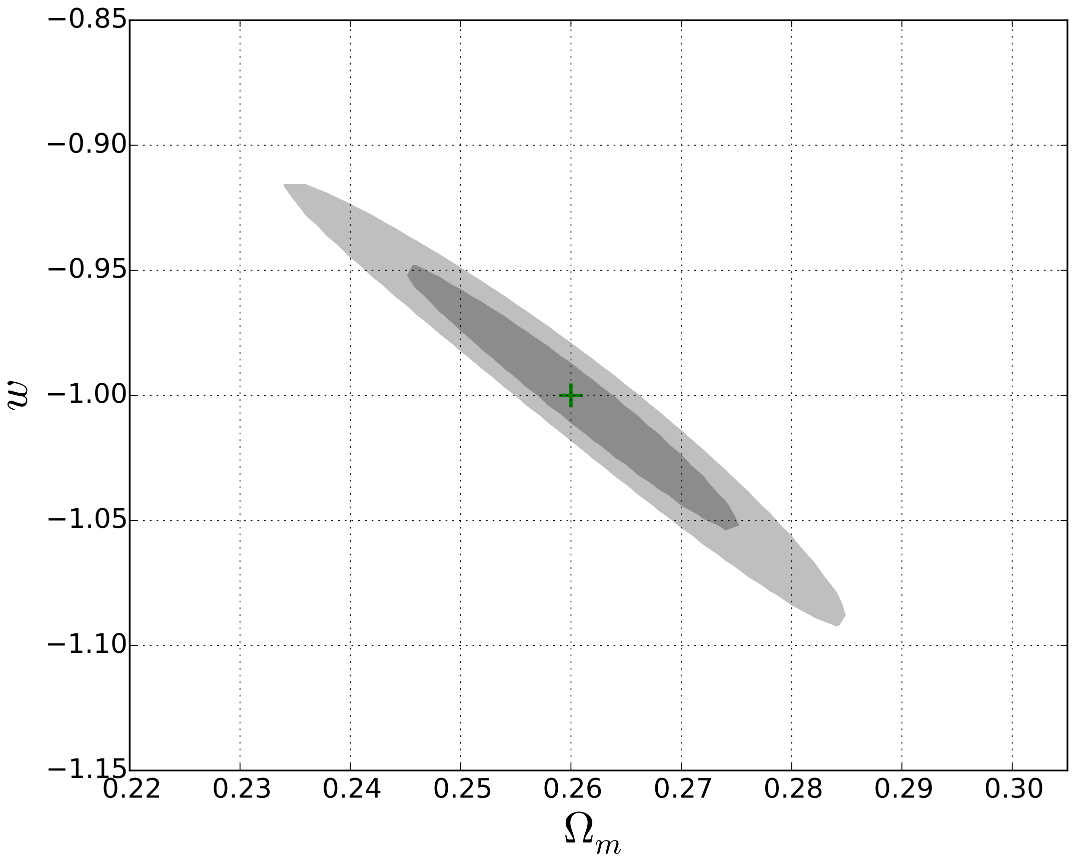

Figure 6. Likelihood contours (68.3%, 95.4%) in the $\Omega_m - w$ plane from our method.

the shape of angular 2pCF is insensitive to redshift in correct cosmology. Our method is complementary to these works in the sense that, we do not require accurate analytic modeling and should be applicable on smaller scales. The two different approaches can be combined together to fully extract the cosmological information.

The method of redshift dependent AP effect has been shown great power to constrain cosmological parameters Li et al. (2014, 2015,?). We hope this method also. The two methods probe different information encoded in the 2pCF and can be combined to fully probe the geometrical effect in LSS. Or one can also use the redshift evolution of 2D 2pCF xi(s,mu) to have all information included.

The method is designed to be applied to current and future LSS surveys, with a particular emphasis to the photometric surveys which probe a large amount of galaxies and the large redshift error will not quite affect the angular 2pCF measurement. An accurate modeling of redshfit error, galaxy bias and RSD effects could be crucial for the successful application of the method. DES will probe 300 million galaxies at $z < 1.4$, and LSST will probe 20 billion galaxies at $z < 2$. We hope our method play an active role in deriving cosmological constraints from LSS surveys.

ACKNOWLEDGMENTS

We thank the Korea Institute for Advanced Study for providing computing resources (KIAS Center for Advanced Computation Linux Cluster System). We would like to thank Yi Zheng for useful discussions. This work was partially supported by the Supercomputing Center/Korea Institute of Science and Technology Information with supercomputing resources including technical support (KSC-2013-G2-003).

APPENDIX

REFERENCES

Ade, P.A.R., Aghanim, N., & Arnaud, M., et al. arXiv:1502.01589
Alam, S., Ata, M., & Bailey, S., et al. 2016, submitted to MNRAS (arXiv:1607.03155)
Alam S., Albareti, F.D.,& Allende Prieto, C., et al., 2015, ApJS, 219, 12
Alcock, C., & Paczynski, B. 1979, Nature, 281, 358
Anderson, L., Aubourg, É., & Bailey, S. et al. 2014, MNRAS, 441, 24
Ballinger, W.E., Peacock, J.A., & Heavens, A.F. 1996, MNRAS, 282, 877
Betoule, M., Kessler, R., & Guy, J., et al. 2014, A&A, 568, 32
Beutler, F., Blake, C., & Colless, M., et al. 2011, MNRAS, 416, 3017
Beutler, F., Saito, S., & Seo, H.-J., et al. 2013, MNRAS, 443, 1065
Beutler, F., Seo, H.-J., & Saito, S., et al. 2016, arXiv:1607.03150
; Blake, C., & Glazebrook, K. 2003, ApJ, 594, 665
Blake, C., Glazebrook, K., & Davis, T. M., 2011, MNRAS, 418, 1725
Blake, C., James, J.B., & Poole, G.B. 2013, MNRAS, 437, 2488
Bolton, A.S., Schlegel, & D.J., Aubourg E., et al. 2012, AJ, 144, 144
Boylan-Kolchin, M., Ma, C.-P., & Quataert, E. 2008, MNRAS, 383, 93
Christensen, N., Meyer, R., Knox, L., & Luey, B. 2001, Class. Quant. Grav., 18, 2677
Chuang, C.-H., & Wang, Y. 2012, MNRAS, 426, 226
Dawson, K.S., Kneib, J.P., & Percival, W.J., et al. 2015, accepted AJ
Dawson, K.S., Schlegel, D.J., & Ahn, C.P., et al. 2012, AJ, 145, 10
Efstathiou, G. 2014, MNRAS, 440, 1138
Eisenstein, D.J., Hu, W., & Tegmark, M. 1998, ApJ, 504, L57
Eisenstein, D.J., Weinberg, D.H., & Agolet, E., et al. 2011, AJ, 142, 72
Feldman, H.A., Kaiser, N., & Peacock, J.A. 1994, ApJ, 426, 23
Fukugita, M., Ichikawa, T., & Gunn, J.E., et al. 1996, AJ, 111, 1748
Gunn, J.E., Carr, M., & Rockosi, C. et al. 1998, AJ, 116, 3040
Gunn, J.E., Siegmund, W.A., & Mannery, E.J., et al. 2006, AJ, 131, 2332
Guzzo, L., Pierleoni, M., & Meneux, B., et al. 2008, Nature, 451, 541
Hartlap J., Simon P. & Schneider P. [astro-ph/0608064].
Hong, S.E., Park, C.,& Kim, J. 2016, ApJ, 823, 103
Jackson, J., 1972, MNRAS, 156, 1
Jennings, E., Baugh, C.M., & Pascoli, S. 2011, MNRAS, 420, 1079
Jeong, D., Dai, L., Kamionkowski, M., & Szalay, A.S. 2014, arXiv:1408.4648
Jiang, C.Y., Jing, Y. P., & Faltenbacher, A., et al. 2008, ApJ, 675, 1095
Kaiser, N. 1987, MNRAS, 227, 1
Kim, J., & Park, C. 2006, ApJ, 639, 600
Kim, J., Park, C., Gott, J.R., III, & Dubinski, J. 2009, ApJ, 701, 1547
Kim, J., Park, C., L'Huillier, B., & Hong, S. E. 2015, JKAS, 48, 213
Kim, J., Park, C., Rossi, G., Lee, S.M., & Gott, J.R. 2011, JKAS, 44, 217
Kitaura, F.S., Rodríguez-Torres, S., Chuang, C.-H., et al. arXiv:1509.06400
Komatsu, E., Smith, K. M., & Dunkley, J., et al. 2011, ApJS, 192, 18
Lacey, C., & Cole, S. 1993, MNRAS, 262, 627
Landy, S.D., & Szalay, A.S. 1993, ApJ, 412, 64
Laureijs, R., Amiaux, J., & Arduini, S., et al. 2011, arXiv:1110.3193
Lavaux, G., & Wandelt, B.D. 2012, ApJ, 754, 109
Lewis, A., & Bridle, S. 2002, Phys. Rev. D, 66, 103511
L'Huillier, B., Park, C., & Kim, J. 2014, New Astronomy, 30, 79
Li, M., Li, X.-D., Wang, S., & Wang, Y. 2011, Commun. Theor. Phys., 56, 525
Li, X.-D., Park, C., Forero-Romero, J., & Kim, J. 2014, ApJ, 796, 137
Li, X.-D., Park, C., Sabiu, C.G., & Kim, J. 2015, MNRAS, 450, 807
Li, X.-D., Park, C., Sabiu, C.G., & Kim, J. 2016, submitted to ApJ
Linder, E.V., Minji, O., Okumura, T., Sabiu, C.G., & Song, Y.-S. 2014, Phys. Rev. D, 89, 063525
López-Corredoira, M. 2014, ApJ, 781, 96
Mao, Q., Berlind, A.A., Scherrer, R.J., et al. 2016, submitted to ApJ
Marinoni, C., & Buzzi, A. 2010, Nature, 468, 539
Matsubara T., & Suto, Y. 1996, ApJ, 470, L1
McCavana, T., Micic, M., Lewis, G. F., et al. 2012, MNRAS, 424, 361
Morandi, A., & Sun, M. arXiv:1601.03741
Outram, P.J., Shanks, T., Boyle, B.J., Croom, S.M., Hoyle, F., Loaring, N.S., Miller, L., & Smith, R.J. 2004, MNRAS, 348, 745
Parejko J.K., et al., 2013, MNRAS, 429, 98
Parihar, P., Vogeley, M.S., & Gott, J.R., et al. 2014, ApJ, 796, 86
Park, C., Kim, J., & Gott, J.R. 2005, ApJ, 633, 1
Park, C., & Kim, Y.-R. 2010, ApJL, 715, L185
Park, C., Choi, Y.-Y., Kim, J., Gott, J.R., Kim, S.S., & Kim, K.-S. 2012, ApJ, 759, 7
Park, C., Song, H., Einasto, M., Lietzen, H., & Heinamaki, P. 2015, JKAS, 48, 75
Peebles, P.J.E., & Ratra, B. 2003, Reviews of Modern Physics, 75, 559
Percival, W.J., Ross, A.J., & Sánchez, A.G., et al. 2014, MNRAS, 439, 2531
Perlmutter, S., Aldering, G., & Goldhaber, G., et al. 1999, ApJ, 517, 565
Press, W.H., & Schechter, P.L. 1974, ApJ, 187, 425

Reid, B., Samushia, L., & White, M., et al. 2012, MNRAS, 426, 2719
Reid, B., Ho, S., & Padmanabhan, N., et al. 2016, MNRAS, 455, 1553
Riess, A.G., Filippenko, A.V., & Challis, P., et al. 1998, AJ, 116, 1009
Riess, A.G., Macri, L., & Casertano, S., et al. 2011, ApJ, 730, 119
Ross, A.J., Percival, W.J., & Sánchez, A.G. et al. 2012, MNRAS, 424, 564
Ross, A.J., Samushia, L., & Howlett, C., et al. 2015, MNRAS, 449, 835
Ryden, B.S. 1995, ApJ, 452, 25
Sutter, P.M., Pisani, A., Wandelt, B.D., & Weinberg, D.H. 2014, MNRAS, 443, 2983
Salvador, S.A., Sánchez, A.G., Padilla, N.D., & Baugh, C.M. 2014, MNRAS, 443, 2612
Salvador, S.A., Sánchez, A.G., & Grieb, J.N., et al. 2016, submitted to MNRAS
Sáchez, A.G., Baugh, C.M., & Percival, W.J. et al. 2006, MNRAS, 366, 187
Sánchez, A. G., Crocce, M., Cabré, A., Baugh, C.M., & Gaztaaga, E. 2009, MNRAS, 400, 1643
Sánchez, A. G., Scoccimarro, R., & Crocce, M., et al. arXiv:1607.03147
Schlafly E.F., Finkbeiner D.P., Schlegel D.J., et al. 2010, ApJ, 725, 1175
Schlafly E.F., & Finkbeiner D.P. 2011, ApJ, 737, 103
Schlegel, D., Abdalla, F., & Abraham, T., et al. 2011, arXiv:1106.1706
Seo, H.-J., & Eisenstein, D.J. 2003, ApJ, 598, 720
Smee, S.A., Gunn, J.E., & Uomoto, A., et al. 2013, AJ, 146, 32
Song, Y.S., Sabiu, C.G., Okumura, T., Oh, M., & Linder, E.V. 2014, JCAP, 12, 005
Speare, R., Gott, J.R., Kim, J., & Park, C. 2015, ApJ, 799, 176
Viana, P.T.P., & Liddle, A.R. 1996, MNRAS, 281, 323
Villalobos, Á., De Lucia, G., Weinmann, S.M., Borgani, S., & Murante, G. 2013, MNRAS, 433, L49
Weinberg, S. 1989, Reviews of Modern Physics, 61, 1
Weinberg, D.H, Mortonson, M.J., Eisenstein, D.J., et al. 2013, Physics Reports, 530, 87
White M., et al. 2011, ApJ, 728, 126
York, D.G., Adelman, J., & Anderson, J.E., et al. 2000, AJ, 120, 1579
Zehavi, I., Zheng, Z., & Weinberg, D.H., et al. 2011, ApJ, 736, 59